

STOCHASTIC INTERPOLANTS WITH DATA-DEPENDENT COUPLINGS

Michael S. Albergo^{*1}, Mark Goldstein^{*2}, Nicholas M. Boffi²,
Rajesh Ranganath^{2,3}, Eric Vanden-Eijnden²

Center for Cosmology and Particle Physics¹, New York University

Courant Institute of Mathematical Sciences², New York University

Center for Data Science³, New York University

albergo@nyu.edu, goldstein@nyu.edu, boffi@cims.nyu.edu,

rajeshr@cims.nyu.edu, eve2@cims.nyu.edu

ABSTRACT

Generative models inspired by dynamical transport of measure – such as flows and diffusions – construct a continuous-time map between two probability densities. Conventionally, one of these is the target density, only accessible through samples, while the other is taken as a simple base density that is data-agnostic. In this work, using the framework of stochastic interpolants, we formalize how to *couple* the base and the target densities. This enables us to incorporate information about class labels or continuous embeddings to construct dynamical transport maps that serve as conditional generative models. We show that these transport maps can be learned by solving a simple square loss regression problem analogous to the standard independent setting. We demonstrate the usefulness of constructing dependent couplings in practice through experiments in super-resolution and in-painting.

1 INTRODUCTION

Generative models such as normalizing flows and diffusions sample from a target density ρ_1 by continuously transforming samples from a base density ρ_0 into the target. This transport is accomplished by means of an Ordinary Differential Equation (ODE) or Stochastic Differential Equation (SDE), which takes as initial condition a sample from ρ_0 and produces at time $t = 1$ an approximate sample from ρ_1 . Typically, the base density is taken to be something simple, analytically tractable, and easy to sample, such as a standard Gaussian. In some formulations, such as score-based diffusion (Sohl-Dickstein et al., 2015; Song & Ermon, 2020; Ho et al., 2020b; Song et al., 2020; Singhal et al., 2023), a Gaussian base density is intrinsically tied to the process achieving the transport. In others, including flow matching (Lipman et al., 2022b; Chen & Lipman, 2023), rectified flow (Liu et al., 2022b; 2023), and stochastic interpolants (Albergo & Vanden-Eijnden, 2022; Albergo et al., 2023), a Gaussian base is not required, but is often chosen for convenience. In these cases, the choice of Gaussian base represents an absence of prior knowledge about the problem structure, and existing works have yet to fully explore the strength of base densities adapted to the target.

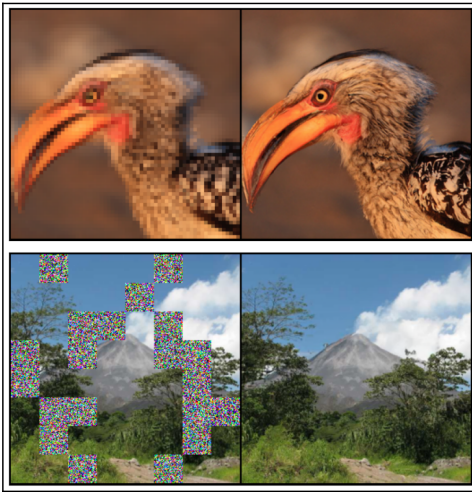


Figure 1: Example results from super-resolution and in-painting applications of stochastic interpolants with data-dependent couplings.

In these cases, the choice of Gaussian base represents an absence of prior knowledge about the problem structure, and existing works have yet to fully explore the strength of base densities adapted to the target.

^{*} Equal Contribution.

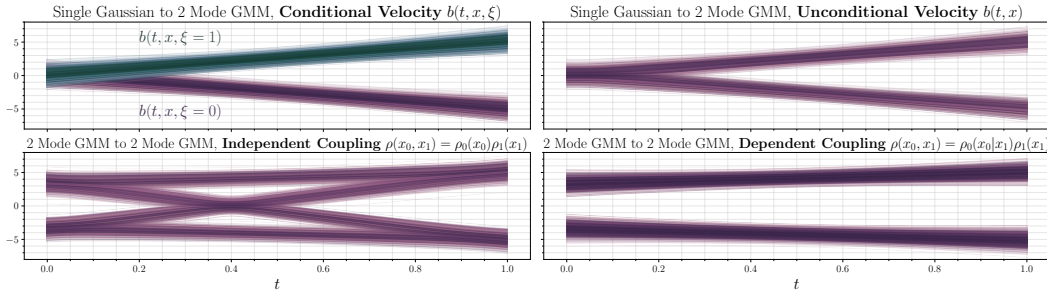


Figure 2: Conditioning and data-dependent coupling. Delineating between conditioning and coupling, and their implications for the corresponding probability flow X_t , as seen in two transport problems. Top row: using a conditional velocity $b(t, x, \xi)$ (left) versus an unconditional velocity $b(t, x)$ (right) to transport a standard Gaussian to a 2-mode Gaussian Mixture Model (PDF). The conditional velocity factorizes into two models, one which maps the whole base ρ_0 to one mode, and one that maps it to the other. Bottom row: flow lines of samples from a 2-mode PDF to another 2-mode PDF, where (left) the coupling of the base and target $\rho(x_0, x_1)$ is independent, and (right) the coupling is conditional on the value of x_1 . The flow lines are straighter, with no formation of auxiliary modes in the intermediate density $\rho(t)$, in juxtaposition to the independent case. This motivates us to consider finding such correlated base variables directly in the data.

In this work, we introduce a general formulation of coupled and conditional base densities, building on the framework of stochastic interpolants. To do so, we introduce the notion of a base density produced via a *coupling*, whereby samples of the base are computed conditionally given samples from the target. We construct a continuous-time stochastic process that interpolates between the coupled base and target, and we characterize the resulting transport by identification of a continuity equation obeyed by the time-dependent density. We show that the velocity field defining this transport can be estimated by solution of an efficient, simulation-free square loss regression problem analogously to standard, data-agnostic interpolant and flow matching algorithms.

In our formulation, we also allow for dependence on an external, conditional source of information independent of ρ_1 . We discuss how this extra source of conditioning can be used to accomplish class-conditional generation, or generation conditioned on a continuous embedding such as a textual representation or problem-specific geometric information. We suggest some generic ways to construct coupled, conditional base and target densities, and we consider practical applications to image super-resolution and in-painting, where we find improved performance by incorporating both a data-dependent coupling and the conditional variable. Together, our **main contributions** can be summarized as:

1. We define a broader way of constructing base and target pairs in generative models based on dynamical transport that adapts the base to the target. In addition, we formalize the use of conditional information – both discrete and continuous – in concert with this new form of *data coupling* in the stochastic interpolant framework. As special cases of our general formulation, we obtain several recent variants of conditional generative models that have appeared in the literature.
2. We provide a characterization of the transport that results from conditional, data-dependent generation, and analyze theoretically how these factors influence the resulting time-dependent density
3. We provide an empirical study on the effect of coupling for stochastic interpolants. Given their recent promise as flexible generative models and the widespread recognition of the importance of conditioning and dependence in generative models, this represents a timely contribution.
4. We demonstrate the utility of data-dependent base densities and the use of conditional information in two canonical applications, image inpainting and super-resolution, which highlight the performance gains that can be obtained through the application of the tools developed here.

The rest of the paper is organized as follows. In [Section 1.1](#), we describe some related work in conditional generative modeling. In [Section 2](#), we introduce our theoretical framework. We characterize the transport that results from the use of data-dependent couplings, and discuss the

Table 1: Couplings. Standard formulations of flows and diffusions construct generative models built upon an independent coupling (Albergo & Vanden-Eijnden, 2022; Albergo et al., 2023; Lipman et al., 2022b; Liu et al., 2022b). Lee et al. (2023) learn $q_\phi(x_0|x_1)$ jointly with the velocity to define the coupling during training, but instead sample from $\rho_0 = \mathcal{N}(0, Id_d)$ for generation. Tong et al. (2023) and Pooladian et al. (2023) build couplings by sampling independently from the base and target and running mini-batch optimal transport algorithms (Cuturi, 2013). Here we focus on couplings enabled by our generic formalism, which can be individualized to each generative task.

Coupling PDF $\rho(x_0, x_1 \xi)$	Base PDF	Description
$\rho_1(x_1)\rho_0(x_0)$	$x_0 \sim \mathcal{N}(0, Id_d)$	Independent
$\rho(x_0 x_1)\rho_1(x_1)$	$x_0 \sim q_\phi(x_0 x_1)$	Learned conditional
mb-OT(x_1, x_0)	$x_0 \sim \mathcal{N}(0, Id_d)$	Minibatch OT
$\rho_1(x_1 \xi)\rho_0(x_0 x_1, \xi)$	$x_0 \sim \mathcal{N}(m(x_1, \xi), C(x_1, \xi))$	Dependent-coupling (this work)

difference between this approach and conditional generative modeling. In Section 3, we apply the framework to numerical experiments on ImageNet, focusing on image inpainting and image super-resolution. We conclude with some remarks and discussion in Section 4.

1.1 RELATED WORKS

Couplings. Several works have studied the question of how to build couplings, primarily from the specific viewpoint of optimal transportation theory. An initial perspective in this regard comes from (Pooladian et al., 2023; Tong et al., 2023; Klein et al., 2023), who state an unbiased means for building entropically-regularized optimal couplings from minibatches of training samples. This perspective is appealing in that it may give probability flows that are straighter and hence more easily computed using simple ODE solvers. However, it relies on estimating an optimal coupling over minibatches of the entire dataset, which, for large datasets, may become uninformative as to the true coupling. In an orthogonal perspective, Lee et al. (2023) presented an algorithm to learn a coupling between the base and the target by building dependence on the target into the base. They argue that this can reduce curvature of the underlying transport. While this perspective allows them to empirically reduce the curvature of the flow lines, it introduces a potential bias in that they still sample from an independent base. Table 1 summarizes these couplings along with the standard independent pairing.

Generative Modeling and Dynamical Transport. Generative models built upon dynamical transport of measure go back at least to (Tabak & Vanden-Eijnden, 2010; Tabak & Turner, 2013), and were further developed in (Rezende & Mohamed, 2015; Dinh et al., 2017; Huang et al., 2016; Durkan et al., 2019) using compositions of discrete maps, while modern models are typically formulated via a continuous-time transformation. In this context, a major advance was the introduction of score-based diffusion (Song et al., 2021b;a), which relates to denoising diffusion probabilistic models (Ho et al., 2020a), and allows one to generate samples by learning to reverse a stochastic differential equation that maps the data into samples from a Gaussian base density. Methods such as flow matching (Lipman et al., 2022a), rectified flow (Liu, 2022; Liu et al., 2022a), and stochastic interpolants (Albergo & Vanden-Eijnden, 2022; Albergo et al., 2023) expand on the idea of building stochastic processes that connect a base density to the target, but allow for bases that are more general than a Gaussian density. Typically, these constructions assume that the samples from the base and the target are uncorrelated.

Conditional Diffusions and Flows for Images. Saharia et al. (2022); Ho et al. (2022a) build diffusions for super-resolution, where low-resolution images are given as inputs to a score model, which formally learns a conditional score (Ho & Salimans, 2022). In-painting can be seen as a form of conditioning where the conditioning set determines some coordinates in the target space. In-painting diffusions have been applied to video generation (Ho et al., 2022b) and protein backbone generation (Trippe et al., 2022). In the *replacement method* one directly inputs the clean values of the known coordinates at each step of integration (Ho et al., 2022b); Schneuing et al. (2022) replace with draws of the diffused state of the known coordinates. Trippe et al. (2022); Wu et al. (2023) discuss approximation error in this approach and correct with sequential Monte-Carlo. We revisit this

problem framing from the velocity modeling perspective in [Section 3.1](#). Recent work has started to apply flows for high dimensional conditional modeling ([Dao et al., 2023](#); [Hu et al., 2023](#)).

2 STOCHASTIC INTERPOLANTS WITH CONDITIONAL COUPLINGS

Suppose that we are given a dataset $\{x_1^i\}_{i=1}^n$, where we allow (but do not require) each data point $x_1^i \in \mathbb{R}^d$ to come with a label $\xi_i \in D$, such as a discrete class or a continuous embedding like a text caption. The aim of a generative model is to draw new samples assuming that the data set comes from a Probability Density Function (PDF) decomposed as $\rho_1(x_1|\xi)\eta(\xi)$, where $\rho_1(x_1|\xi)$ is the density of the data x_1 conditioned on their label ξ , and $\eta(\xi)$ is the density of the label. In the following, we will somewhat abuse notation and use $\eta(\xi)$ even when ξ is discrete (in which case, $\eta(\xi)$ is a sum of Dirac measures); we will however assume that $\rho_1(x_1|\xi)$ is a proper density. Following the stochastic interpolant framework ([Albergo & Vanden-Eijnden, 2022](#); [Albergo et al., 2023](#)), we introduce a time-dependent stochastic process that interpolates between samples from a simple base density $\rho_0(x_0|\xi)$ at time $t = 0$ and samples from the target $\rho_1(x_1|\xi)$ at time $t = 1$:

Definition 1 (Stochastic interpolant with coupling). *The stochastic interpolant x_t is the stochastic process defined as¹*

$$x_t = \alpha(t)x_0 + \beta(t)x_1 + \gamma(t)z \quad t \in [0, 1], \quad (1)$$

where

- $\alpha(t)$, $\beta(t)$, and $\gamma^2(t)$ are differentiable functions of time such that $\alpha(0) = \beta(1) = 1$, $\alpha(1) = \beta(0) = \gamma(0) = \gamma(1) = 0$, and $\alpha^2(t) + \beta^2(t) + \gamma^2(t) > 0$ for all $t \in [0, 1]$.
- The pair (x_0, x_1) are jointly drawn from a conditional probability density $\rho(x_0, x_1|\xi)$ such that

$$\int_{\mathbb{R}^d} \rho(x_0, x_1|\xi) dx_1 = \rho_0(x_0|\xi), \quad \int_{\mathbb{R}^d} \rho(x_0, x_1|\xi) dx_0 = \rho_1(x_1|\xi). \quad (2)$$

- $z \sim \mathcal{N}(0, Id)$, independent of (x_0, x_1, ξ) .

A simple instance of (1) uses $\alpha(t) = 1 - t$, $\beta(t) = t$, and $\gamma(t) = \sqrt{2t(1-t)}$.

The stochastic interpolant framework uses information about the process x_t to derive either an ODE or SDE whose solutions X_t push the law of x_0 onto the law of x_t for all times $t \in [0, 1]$.

As shown in [Section 2.1](#), the drift coefficients in these ODEs/SDEs can be estimated by quadratic regression. They can then be used as generative models, owing to the property that the process x_t specified in [Definition 1](#) satisfies $x_{t=0} = x_0 \sim \rho_0(x_0|\xi)$ and $x_{t=1} = x_1 \sim \rho_1(x_1|\xi)$, and hence samples the desired target density. By drawing samples $x_0 \sim \rho_0(x_0|\xi)$ and using them as initial data $X_{t=0} = x_0$ in the ODEs/SDEs, we can then generate samples $X_{t=1} \sim \rho_1(x_1|\xi)$ via numerical integration.

In the original papers, this construction was made using the choice $\rho(x_0, x_1|\xi) = \rho_0(x_0)\rho_1(x_1)$, so that x_0 and x_1 were drawn independently from the base and the target, and the label ξ was not used.

Our aim here is to explore and exploit, via suitable definition of $\rho(x_0, x_1|\xi)$, dependent couplings between x_0 and x_1 to build generative models that are more powerful and versatile.

Before doing so, we first explain how to build generative models based on the stochastic interpolants in [Definition 1](#) given any $\rho(x_0, x_1|\xi)$.

2.1 TRANSPORT EQUATIONS AND CONDITIONAL GENERATIVE MODELS

In this section, we show that the probability distribution of the process x_t defined in (1) has a time-dependent density $\rho(t, x|\xi)$ that interpolates between $\rho_0(x|\xi)$ and $\rho_1(x|\xi)$. We characterize this

¹More generally, we may set $x_t = I(t, x_0, x_1)$ in (1), where I satisfies some regularity properties in addition to the boundary conditions $I(t = 0, x_0, x_1) = x_0$ and $I(t = 1, x_0, x_1) = x_1$ ([Albergo & Vanden-Eijnden, 2022](#); [Albergo et al., 2023](#)). For simplicity, we will stick to the linear choice $I(t, x_0, x_1) = \alpha(t)x_0 + \beta(t)x_1$.

density as the solution of a transport equation, and we show that both the corresponding velocity field and the score $\nabla \log \rho(t, x|\xi)$ are minimizers of simple quadratic objective functions.

This result enables us to construct conditional generative models by approximating the velocity (and possibly the score) via minimization over a rich parametric class such as neural networks. We first define the functions

$$g_0(t, x, \xi) = \mathbb{E}(x_0|x_t = x), \quad g_1(t, x, \xi) = \mathbb{E}(x_1|x_t = x), \quad g_z(t, x, \xi) = \mathbb{E}(z|x_t = x) \quad (3)$$

where $\mathbb{E}(\cdot|x_t = x)$ denotes the expectation over $\rho(x_0, x_1|\xi)$ conditional on $x_t = x$. We then have,

Theorem 1 (Transport equation). *The probability distribution of the stochastic interpolant x_t defined in (1) has a density $\rho(t, x|\xi)$ that satisfies $\rho(t = 0, x|\xi) = \rho_0(x|\xi)$ and $\rho(t = 1, x|\xi) = \rho_1(x|\xi)$, and solves the transport equation*

$$\partial_t \rho(t, x|\xi) + \nabla \cdot (b(t, x, \xi)\rho(t, x|\xi)) = 0, \quad (4)$$

where the velocity field can be written as

$$b(t, x, \xi) = \dot{\alpha}(t)g_0(t, x, \xi) + \dot{\beta}(t)g_1(t, x, \xi) + \dot{\gamma}(t)g_z(t, x, \xi). \quad (5)$$

Moreover, for every t such that $\gamma(t) \neq 0$, the following identity for the score holds

$$\nabla \log \rho(t, x|\xi) = -\gamma^{-1}(t)g_z(t, x, \xi). \quad (6)$$

The functions g_0 , g_1 , and g_z are the unique minimizers of the objectives

$$\begin{aligned} L_0(\hat{g}_0) &= \int_0^1 \mathbb{E} [|\hat{g}_0(t, x_t, \xi)|^2 - 2x_0 \cdot \hat{g}_0(t, x_t, \xi)] dt, \\ L_1(\hat{g}_1) &= \int_0^1 \mathbb{E} [|\hat{g}_1(t, x_t, \xi)|^2 - 2x_1 \cdot \hat{g}_1(t, x_t, \xi)] dt, \\ L_z(\hat{g}_z) &= \int_0^1 \mathbb{E} [|\hat{g}_z(t, x_t, \xi)|^2 - 2z \cdot \hat{g}_z(t, x_t, \xi)] dt, \end{aligned} \quad (7)$$

where \mathbb{E} denotes an expectation over $(x_0, x_1) \sim \rho(x_0, x_1|\xi)$, $\xi \sim \eta(\xi)$, and $z \sim \mathcal{N}(0, Id)$.

This result is proven in [Appendix A](#). The objectives (7) can readily be estimated in practice from samples $(x_0, x_1) \sim \rho(x_0, x_1|\xi)$, $z \sim \mathcal{N}(0, 1)$, and $\xi \sim \eta(\xi)$, which will enable us to learn approximations for use in a generative model. Moreover, because $\mathbb{E}(x_t|x_t = x) = x$ by definition, the functions g_0 , g_1 , and g_z satisfy for every t , x , and ξ ,

$$\alpha(t)g_0(t, x, \xi) + \beta(t)g_1(t, x, \xi) + \gamma(t)g_z(t, x, \xi) = x. \quad (8)$$

This enables us to reduce computational expense: given two of the g 's, the third can always be calculated via (8). The transport equation (4) can be used to derive generative models, as we now show.

Corollary 2 (Probability flow and diffusions). *The solutions to the probability flow equation*

$$\dot{X}_t = b(t, X_t, \xi) \quad (9)$$

enjoy the property that

$$X_{t=1} \sim \rho_1(x_1|\xi) \quad \text{if} \quad X_{t=0} \sim \rho_0(x_0|\xi) \quad (10)$$

$$X_{t=0} \sim \rho_0(x_0|\xi) \quad \text{if} \quad X_{t=1} \sim \rho_1(x_1|\xi) \quad (11)$$

In addition, for any $\epsilon(t) \geq 0$, solutions to the forward SDE

$$dX_t^F = b(t, X_t^F, \xi)dt - \epsilon(t)\gamma^{-1}(t)g_z(t, X_t^F, \xi)dt + \sqrt{2\epsilon(t)}dW_t, \quad (12)$$

enjoy the property that

$$X_{t=1}^F \sim \rho_1(x_1|\xi) \quad \text{if} \quad X_{t=0}^F \sim \rho_0(x_0|\xi), \quad (13)$$

and solutions to the backward SDE

$$dX_t^R = b(t, X_t^R, \xi)dt + \epsilon(t)\gamma^{-1}(t)g_z(t, X_t^R, \xi)dt + \sqrt{2\epsilon(t)}dW_t, \quad (14)$$

enjoy the property that

$$X_{t=0}^R \sim \rho_0(x_0|\xi) \quad \text{if} \quad X_{t=1}^R \sim \rho_1(x_1|\xi). \quad (15)$$

This result is proven in [Appendix A](#). Note that if we additionally draw ξ marginally from $\eta(\xi)$ when we generate the solution to these equations, we can also generate samples from the unconditional $\rho_0(x_0) = \int_D \rho_0(x_0|\xi)\eta(\xi)d\xi$ and $\rho_1(x_1) = \int_D \rho_1(x_1|\xi)\eta(\xi)d\xi$.

Let us now discuss two generic instantiations our formalism, corresponding to either class conditioning alone or class conditioning with dependent coupling. These examples will emphasize the differences between the two choices and will make clear the added advantage of employing data-dependent coupling in concert with class conditioning. We show a pictorial representation of the two instantiations in [Fig. 2](#), highlighting the differences in the resulting flows.

2.2 CLASS CONDITIONING

Class conditioning alone amounts to a new choice of the target density, so that

$$\rho(x_0, x_1|\xi) = \rho_0(x_0)\rho_1(x_1|\xi). \quad (16)$$

To learn in this setup, we can evaluate the objective functions (7) over a minibatch of $n_b < n$ pairs (x_1^i, ξ_i) using an additional n_b samples $x_0^i \sim \rho_0(x_0)$, $z_i \sim \mathcal{N}(0, Id)$, and $t_i \sim U([0, 1])$. This leads to the empirical approximation \hat{L}_0 of L_0

$$\hat{L}_0(\hat{g}_0) = \frac{1}{n_b} \sum_{i=1}^{n_b} [|\hat{g}_0(x_i, \xi_i)|^2 - 2x_0^i \cdot \hat{g}_0(x_i, \xi_i)], \quad (17)$$

with similar empirical variants of L_1 and L_z . In (17), $x_i = \alpha(t_i)x_0^i + \beta(t_i)x_1^i + \gamma(t_i)z_i$. If we approximate the functions $g_0(t, x, \xi)$, $g_1(t, x, \xi)$, and $g_z(t, x, \xi)$ using a rich parametric class such as a set of neural networks, these empirical objectives can be minimized with respect to the parameters using an algorithm such as stochastic gradient descent. This leads to an approximation of the velocity $b(t, x, \xi)$ via (5) and an approximation of the score via (6). To generate new samples conditioned on a given class ξ , we can draw a random $x_0 \sim \rho_0(x_0)$ and use it as an initial condition in the probability flow ODE (9) or the forward SDE (12) to produce $X_{t=1} \sim \rho_1(x_1|\xi)$ or $X_{t=1}^F \sim \rho_1(x_1|\xi)$. Here, the conditioning arises because the learned velocity field $b(t, x, \xi)$ and score depend on ξ .

2.3 DATA-DEPENDENT COUPLING

In [Section 2.2](#), we consider a setting in which the base density ρ_0 is independent of the target ρ_1 . Here, we extend this setup to allow for a data-dependent coupling between the base and the target. To do so, we set

$$\rho(x_0, x_1|\xi) = \rho_1(x_1|\xi)\rho_0(x_0|x_1, \xi) \quad \text{with} \quad \int_{\mathbb{R}^d} \rho_0(x_0|x_1, \xi)\rho_1(x_1|\xi)dx_1 = \rho_0(x_0|\xi). \quad (18)$$

There are many ways to construct the conditional $\rho_0(x_0|x_1, \xi)$. In the numerical experiments in [Section 3.1](#) & [Section 3.2](#), we consider base densities of the generic form

$$\rho_0(x_0|x_1, \xi) = \mathcal{N}(x_0; m(x_1, \xi), C(x_1, \xi)), \quad (19)$$

where the mean $m(x_1, \xi) \in \mathbb{R}^d$ and covariance $C(x_1, \xi) \in \mathbb{R}^{d \times d}$ may both depend on x_1 and ξ . Intuitively, the choice (19) constructs a coupling between samples x_0 and x_1 by applying a deterministic map to x_1 and corrupting the result with Gaussian noise whose variance also depends on x_1 . A simple example is given by $m(x_1^i, \xi) = x_1^i$ and $C(x_1, \xi) = \sigma^2 Id$ for some $\sigma > 0$, which sets the base distribution to be a noisy version of the target.

In practice, we can evaluate the objective functions (7) via the estimator (17) with a minibatch of $n_b < n$ pairs (x_1^i, ξ_i) and an additional n_b samples $z_i \sim \mathcal{N}(0, Id)$ and $t_i \sim U([0, 1])$. We then set

$$x_0^i = m(x_1^i, \xi) + \sigma(x_1^i, \xi_i)\zeta_i, \quad (20)$$

with $\zeta_i \sim \mathcal{N}(0, Id_d)$ and $\sigma(x_1, \xi)\sigma^\top(x_1, \xi) = C(x_1, \xi)$. The rest of the learning procedure follows [Section 2.2](#).

Generating data requires sampling an $X_{t=0} \sim \rho_0(x_0|\xi)$ as an initial condition to be evolved via the probability flow ODE (9) or the forward SDE (12) to respectively produce a sample $X_{t=1} \sim \rho_1(x_1|\xi)$ or $X_{t=1}^F \sim \rho_1(x_1|\xi)$. Sampling an x_0 can be performed by picking a pair (x_1, ξ) either from the data

set or from some online data acquisition procedure and using it in (20). The generated samples from either the probability flow ODE or forward SDE will be different from x_1 , even with the choices $m(x_1, \xi) = x_1$ and $C(x_1, \xi) = \sigma^2 Id$. The probability flow ODE necessarily produces a single sample for each x_0 , while the SDE produces a collection of samples whose spread can be controlled by the diffusion coefficient $\epsilon(t)$.

3 NUMERICAL EXPERIMENTS

We now explore the proposed interpolant framework with dependent couplings on conditional image generation tasks; we find that the framework is straightforward to scale to high resolution images in pixel space.

3.1 IN-PAINTING

We consider an in-painting task, whereby $x_1 \in \mathbb{R}^{C \times W \times H}$ denotes an image with C channels, width W , and height H . Given a pre-specified mask, the goal is to fill the pixels in the masked region with new values that are consistent with the entirety of the image. To fit this problem within our data-dependent coupling framework, we set the conditioning variable $\xi \in \{0, 1\}^{C \times W \times H}$ equal to the mask. For simplicity, we fix the values of the mask across channels, so that it corresponds to masking a specific region of the image in a channel-independent fashion. We define the base density by the relation $x_0 = \xi \circ x_1 + (1 - \xi) \circ \zeta$, where \circ denotes the Hadamard (elementwise) product and $\zeta \in \mathbb{R}^{C \times W \times H}$, $\zeta \sim \mathcal{N}(0, Id)$ denotes random white-noise values used to corrupt the pixels within the masked region. Unlike the mask, these noise values can vary across channels. The spatial structure of the mask is drawn randomly by tiling the image into 64 tiles; each tile is selected to enter the mask with probability $p = 0.3$. In our experiments, we set $\rho_1(x_1)$ to correspond to either Imagenet-256 or Imagenet-512. This corresponds to using $\rho(x_0, x_1 | \xi) = \rho_1(x_1) \rho_0(x_0 | x_1, \xi)$, which informs the model both of the masked regions and initializes the sample from the corrupted image. In the interpolant (1), we set $\alpha(t) = t$ and $\beta(t) = 1 - t$.

Masking the vector field output In this setup, the optimal velocity field $b(x, t, \xi) = b^*(x, t) \circ (1 - \xi)$ for a mask-independent velocity b^* . This follows because $\xi \circ x_t = \xi \circ x_1$ for every t , i.e., the unmasked pixels in x_t are always those of x_1 . To take this structural information into account, we can build this property into our neural network model, and mask the output of the approximate velocity field to enforce that the unmasked pixels remain fixed.

Results For implementation we learn a velocity model $b(x, t, y, \xi)$ where y is the imagenet class label and ξ is the missingness mask. In practice we append ξ to the channels of the inputs x which requires no modification to the basic Unet architecture from Ho et al. (2020b). Additional specific experimental details may be found in Appendix B. The results are in Figure 3 and Figure 4, as well as Section 1. As discussed, the missing areas of the image are defined at time zero as independent normal random variables, depicted as colorful static in the images. In each image triple, the left panel is the base distribution sample x_0 , the middle is the model sample of $X_{t=1}$ obtained by integrated the probability flow ODE (9), and the right panel is the ground truth. The generated textures, though different from the full sample, correspond to realistic samples from the conditional densities given the observed content.

3.2 SUPER-RESOLUTION ON IMAGENET

We now consider image super-resolution, in which we wish to take an image and convert it into an equivalent image at higher resolution. To this end, we let $x_1 \in \mathbb{R}^{C \times \tilde{W} \times \tilde{H}}$ correspond to a high-resolution image, as in Section 3.1. We denote by $\mathcal{D} : \mathbb{R}^{C \times W \times H} \rightarrow \mathbb{R}^{C \times W_{\text{low}} \times H_{\text{low}}}$ and $\mathcal{U} : \mathbb{R}^{C \times W_{\text{low}} \times H_{\text{low}}} \rightarrow \mathbb{R}^{C \times W \times H}$ image downsampling and upsampling operations, where W_{low} and H_{low} denote the width and height of a low-resolution image. To define the base density, we then set $x_0 = \mathcal{U}(\mathcal{D}(x_1)) + \sigma \zeta$ with $\zeta \in \mathbb{R}^{C \times W \times H}$, $\zeta \sim \mathcal{N}(0, Id)$, and $\sigma > 0$. Defining x_0 in this way frames the transport problem such that each starting pixel is proximal to its intended target. Notice in particular that, with $\sigma = 0$, each x_0 would correspond to a lower-dimensional sample embedded in a higher-dimensional space, and the corresponding distribution would be concentrated on a lower-dimensional manifold. Working with $\sigma > 0$ allows us to alleviate the associated singularities by

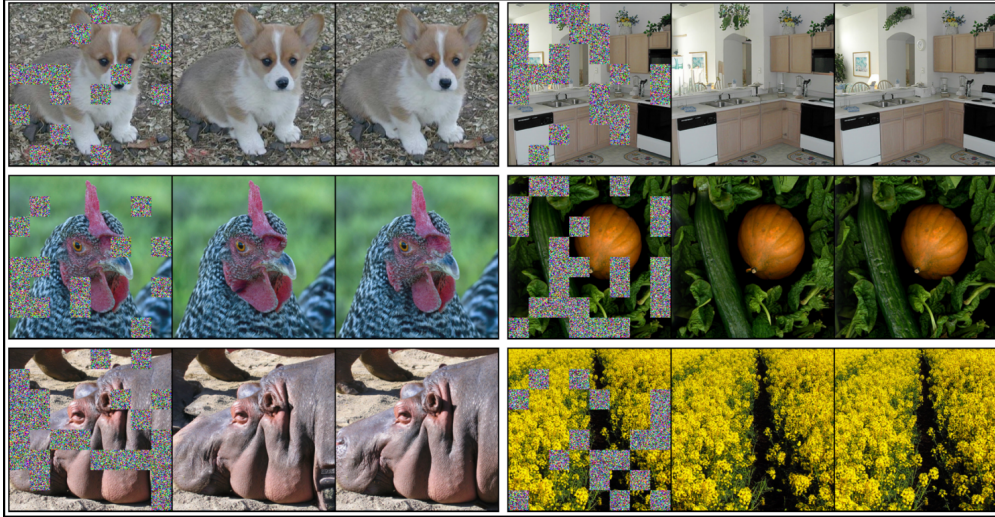


Figure 3: Image inpainting: ImageNet- 256×256 . Six examples of image in-filling, where the left columns display masked images, the center corresponds to in-filled model samples, and the right shows full reference images. In this task, one does not hope to recover the precise content of the reference image, but instead, only a plausible in-filling according to the conditional distribution of the data.



Figure 4: Inpainting: ImageNet- 512×512 . Four examples of image in-filling, as described in Fig. 3, on higher-resolution 512×512 images.

adding a small amount of Gaussian noise to smooth the base density so it is well-defined over the entire higher-dimensional ambient space. In addition, we give the model access to the low-resolution image at all times; this problem setting then corresponds to using $\rho(x_0, x_1|\xi) = \rho_1(x_1)\rho_0(x_0|x_1, \xi)$ with $\xi = \mathcal{U}(\mathcal{D}(x_1))$. In the experiments, we set $\alpha(t) = t$ and $\beta(t) = 1 - t$, and we set ρ_1 to correspond to ImageNet-256 or ImageNet-512, following prior work (Saharia et al., 2022; Ho et al., 2022a).

Results Similarly to the previous experiment, we append the upsampled low-resolution images ξ to the channel dimension of the input x of the velocity model, and likewise include the Imagenet class labels y . The results are in Fig. 5 and Fig. 6, as well as Section 1. Similar in layout to the previous experiment, the left panel of each triplet is the low-resolution image, the middle panel is the model sample $X_{t=1}$, and the right panel is the high-resolution image. The differences are easiest to see when zoomed-in. While the resolution increase from the model is very noticeable for 64 to 256, the differences even in ground truth images between 256 and 512 are more subtle.



Figure 5: Super-resolution: $64 \times 64 \mapsto 256 \times 256$. Super-resolved images where the left-most image is the lower resolution version, the middle is the model output, and the right is the ground truth.



Figure 6: Super-resolution: $256 \times 256 \mapsto 512 \times 512$. Super-resolved images where the left-most image is the lower resolution version, the middle is the model output, and the right is the ground truth. The images are best viewed zoomed-in.

4 DISCUSSION, CHALLENGES, AND FUTURE WORK

In this work, we introduced a general framework for constructing data-dependent couplings between the base and target densities within the stochastic interpolant formalism. In addition, we highlighted how conditional information can be incorporated into the resulting transport by modifying both the

base and the target. Dependent non-Gaussian base distributions have been explored implicitly in diffusion works that forego the stochastic differential equation formalism and stationary distribution requirements in place of general corruptions (Daras et al., 2022; Bansal et al., 2022), where generation can start from corrupted images; this motivates directly stating the modeling problem to start at such corruption, or more generally correlated base variables. We provide some suggestions for specific forms of data-dependent coupling, such as choosing for ρ_0 a Gaussian distribution with mean and covariance adapted to samples from the target, and showed how they can be used in practical problem settings such as image inpainting and super-resolution. There are many interesting generative modeling problems that stand to benefit from the incorporation of data-dependent structure. In the sciences, one potential application is in molecule generation, where we can imagine using data-dependent base distributions to fix a chemical backbone and vary functional groups. The dependency and conditioning structure needed to accomplish a task like this is similar to image inpainting. In machine learning, one potential application is in correcting autoencoding errors produced by an architecture such as a variational autoencoder (Kingma & Welling, 2013), where we could take the target density to be inputs to the autoencoder and the base density to be the output of the autoencoder.

REFERENCES

- Michael S Albergo and Eric Vanden-Eijnden. Building normalizing flows with stochastic interpolants. *arXiv preprint arXiv:2209.15571*, 2022.
- Michael S Albergo, Nicholas M Boffi, and Eric Vanden-Eijnden. Stochastic interpolants: A unifying framework for flows and diffusions. *arXiv preprint arXiv:2303.08797*, 2023.
- Arpit Bansal, Eitan Borgnia, Hong-Min Chu, Jie S Li, Hamid Kazemi, Furong Huang, Micah Goldblum, Jonas Geiping, and Tom Goldstein. Cold diffusion: Inverting arbitrary image transforms without noise. *arXiv preprint arXiv:2208.09392*, 2022.
- Ricky T. Q. Chen. torchdiffeq, 2018. URL <https://github.com/rtqichen/torchdiffeq>.
- Ricky TQ Chen and Yaron Lipman. Riemannian flow matching on general geometries. *arXiv preprint arXiv:2302.03660*, 2023.
- Marco Cuturi. Sinkhorn distances: Lightspeed computation of optimal transport. *Advances in neural information processing systems*, 26, 2013.
- Quan Dao, Hao Phung, Binh Nguyen, and Anh Tran. Flow matching in latent space. *arXiv preprint arXiv:2307.08698*, 2023.
- Giannis Daras, Mauricio Delbracio, Hossein Talebi, Alexandros G Dimakis, and Peyman Milanfar. Soft diffusion: Score matching for general corruptions. *arXiv preprint arXiv:2209.05442*, 2022.
- Laurent Dinh, Jascha Sohl-Dickstein, and Samy Bengio. Density Estimation Using Real NVP. In *International Conference on Learning Representations*, pp. 32, 2017.
- Conor Durkan, Artur Bekasov, Iain Murray, and George Papamakarios. Neural spline flows. In H. Wallach, H. Larochelle, A. Beygelzimer, F. d'Alché-Buc, E. Fox, and R. Garnett (eds.), *Advances in Neural Information Processing Systems*, volume 32. Curran Associates, Inc., 2019. URL <https://proceedings.neurips.cc/paper/2019/file/7ac71d433f282034e088473244df8c02-Paper.pdf>.
- Jonathan Ho and Tim Salimans. Classifier-free diffusion guidance. *arXiv preprint arXiv:2207.12598*, 2022.
- Jonathan Ho, Ajay Jain, and Pieter Abbeel. Denoising diffusion probabilistic models. In H. Larochelle, M. Ranzato, R. Hadsell, M.F. Balcan, and H. Lin (eds.), *Advances in Neural Information Processing Systems*, volume 33, pp. 6840–6851. Curran Associates, Inc., 2020a. URL <https://proceedings.neurips.cc/paper/2020/file/4c5bcbfec8584af0d967f1ab10179ca4b-Paper.pdf>.
- Jonathan Ho, Ajay Jain, and Pieter Abbeel. Denoising diffusion probabilistic models. *Advances in neural information processing systems*, 33:6840–6851, 2020b.

- Jonathan Ho, Chitwan Saharia, William Chan, David J Fleet, Mohammad Norouzi, and Tim Salimans. Cascaded diffusion models for high fidelity image generation. *The Journal of Machine Learning Research*, 23(1):2249–2281, 2022a.
- Jonathan Ho, Tim Salimans, Alexey Gritsenko, William Chan, Mohammad Norouzi, and David J Fleet. Video diffusion models. *arXiv:2204.03458*, 2022b.
- Vincent Tao Hu, David W Zhang, Meng Tang, Pascal Mettes, Deli Zhao, and Cees GM Snoek. Latent space editing in transformer-based flow matching. In *ICML Workshop on New Frontiers in Learning, Control, and Dynamical Systems*, 2023.
- Gao Huang, Yu Sun, Zhuang Liu, Daniel Sedra, and Kilian Weinberger. Deep Networks with Stochastic Depth. *arXiv:1603.09382 [cs]*, July 2016.
- Diederik P Kingma and Jimmy Ba. Adam: A method for stochastic optimization. *arXiv preprint arXiv:1412.6980*, 2014.
- Diederik P Kingma and Max Welling. Auto-Encoding Variational Bayes. *arXiv [Preprint]*, 0, 2013. URL <https://arxiv.org/1312.6114v10>.
- Leon Klein, Andreas Krämer, and Frank Noé. Equivariant flow matching, 2023.
- Sangyun Lee, Beomsu Kim, and Jong Chul Ye. Minimizing trajectory curvature of ode-based generative models. *arXiv preprint arXiv:2301.12003*, 2023.
- Yaron Lipman, Ricky T. Q. Chen, Heli Ben-Hamu, Maximilian Nickel, and Matt Le. Flow matching for generative modeling, 2022a. URL <https://arxiv.org/abs/2210.02747>.
- Yaron Lipman, Ricky TQ Chen, Heli Ben-Hamu, Maximilian Nickel, and Matt Le. Flow matching for generative modeling. *arXiv preprint arXiv:2210.02747*, 2022b.
- Qiang Liu. Rectified flow: A marginal preserving approach to optimal transport, 2022. URL <https://arxiv.org/abs/2209.14577>.
- Xingchao Liu, Chengyue Gong, and Qiang Liu. Flow straight and fast: Learning to generate and transfer data with rectified flow, 2022a. URL <https://arxiv.org/abs/2209.03003>.
- Xingchao Liu, Chengyue Gong, and Qiang Liu. Flow straight and fast: Learning to generate and transfer data with rectified flow. *arXiv preprint arXiv:2209.03003*, 2022b.
- Xingchao Liu, Xiwen Zhang, Jianzhu Ma, Jian Peng, and Qiang Liu. InstafLOW: One step is enough for high-quality diffusion-based text-to-image generation. *arXiv preprint arXiv:2309.06380*, 2023.
- Aram-Alexandre Pooladian, Heli Ben-Hamu, Carles Domingo-Enrich, Brandon Amos, Yaron Lipman, and Ricky Chen. Multisample flow matching: Straightening flows with minibatch couplings. *arXiv preprint arXiv:2304.14772*, 2023.
- Danilo Rezende and Shakir Mohamed. Variational Inference with Normalizing Flows. In *International Conference on Machine Learning*, pp. 1530–1538. PMLR, June 2015.
- Chitwan Saharia, Jonathan Ho, William Chan, Tim Salimans, David J Fleet, and Mohammad Norouzi. Image super-resolution via iterative refinement. *IEEE Transactions on Pattern Analysis and Machine Intelligence*, 45(4):4713–4726, 2022.
- Arne Schneuing, Yuanqi Du, Charles Harris, Arian Jamasb, Ilia Igashov, Weitao Du, Tom Blundell, Pietro Lió, Carla Gomes, Max Welling, et al. Structure-based drug design with equivariant diffusion models. *arXiv preprint arXiv:2210.13695*, 2022.
- Raghav Singhal, Mark Goldstein, and Rajesh Ranganath. Where to diffuse, how to diffuse, and how to get back: Automated learning for multivariate diffusions. In *The Eleventh International Conference on Learning Representations*, 2023.
- Jascha Sohl-Dickstein, Eric Weiss, Niru Maheswaranathan, and Surya Ganguli. Deep unsupervised learning using nonequilibrium thermodynamics. In *International conference on machine learning*, pp. 2256–2265. PMLR, 2015.

- Yang Song and Stefano Ermon. Improved techniques for training score-based generative models. *Advances in neural information processing systems*, 33:12438–12448, 2020.
- Yang Song, Jascha Sohl-Dickstein, Diederik P Kingma, Abhishek Kumar, Stefano Ermon, and Ben Poole. Score-based generative modeling through stochastic differential equations. *arXiv preprint arXiv:2011.13456*, 2020.
- Yang Song, Conor Durkan, Iain Murray, and Stefano Ermon. Maximum likelihood training of score-based diffusion models. In M. Ranzato, A. Beygelzimer, Y. Dauphin, P.S. Liang, and J. Wortman Vaughan (eds.), *Advances in Neural Information Processing Systems*, volume 34, pp. 1415–1428. Curran Associates, Inc., 2021a. URL <https://proceedings.neurips.cc/paper/2021/file/0a9fdbb17feb6ccb7ec405cfb85222c4-Paper.pdf>.
- Yang Song, Jascha Sohl-Dickstein, Diederik P Kingma, Abhishek Kumar, Stefano Ermon, and Ben Poole. Score-based generative modeling through stochastic differential equations. In *International Conference on Learning Representations*, 2021b.
- E. G. Tabak and Cristina V. Turner. A family of nonparametric density estimation algorithms. *Communications on Pure and Applied Mathematics*, 66(2):145–164, 2013. doi: <https://doi.org/10.1002/cpa.21423>. URL <https://onlinelibrary.wiley.com/doi/abs/10.1002/cpa.21423>.
- Esteban G. Tabak and Eric Vanden-Eijnden. Density estimation by dual ascent of the log-likelihood. *Communications in Mathematical Sciences*, 8(1):217–233, 2010. ISSN 15396746, 19450796. doi: 10.4310/CMS.2010.v8.n1.a11.
- Alexander Tong, Nikolay Malkin, Guillaume Huguette, Yanlei Zhang, Jarrid Rector-Brooks, Kilian Fatras, Guy Wolf, and Yoshua Bengio. Improving and generalizing flow-based generative models with minibatch optimal transport. In *ICML Workshop on New Frontiers in Learning, Control, and Dynamical Systems*, 2023.
- Brian L Trippe, Jason Yim, Doug Tischer, David Baker, Tamara Broderick, Regina Barzilay, and Tommi Jaakkola. Diffusion probabilistic modeling of protein backbones in 3d for the motif-scaffolding problem. *arXiv preprint arXiv:2206.04119*, 2022.
- Luhuan Wu, Brian L Trippe, Christian A Naesseth, David M Blei, and John P Cunningham. Practical and asymptotically exact conditional sampling in diffusion models. *arXiv preprint arXiv:2306.17775*, 2023.

A OMITTED PROOFS

Theorem 1 (Transport equation). *The probability distribution of the stochastic interpolant x_t defined in (1) has a density $\rho(t, x|\xi)$ that satisfies $\rho(t = 0, x|\xi) = \rho_0(x|\xi)$ and $\rho(t = 1, x|\xi) = \rho_1(x|\xi)$, and solves the transport equation*

$$\partial_t \rho(t, x|\xi) + \nabla \cdot (b(t, x, \xi) \rho(t, x|\xi)) = 0, \quad (4)$$

where the velocity field can be written as

$$b(t, x, \xi) = \dot{\alpha}(t)g_0(t, x, \xi) + \dot{\beta}(t)g_1(t, x, \xi) + \dot{\gamma}(t)g_z(t, x, \xi). \quad (5)$$

Moreover, for every t such that $\gamma(t) \neq 0$, the following identity for the score holds

$$\nabla \log \rho(t, x|\xi) = -\gamma^{-1}(t)g_z(t, x, \xi). \quad (6)$$

The functions g_0 , g_1 , and g_z are the unique minimizers of the objectives

$$\begin{aligned} L_0(\hat{g}_0) &= \int_0^1 \mathbb{E} [|\hat{g}_0(t, x_t, \xi)|^2 - 2x_0 \cdot \hat{g}_0(t, x_t, \xi)] dt, \\ L_1(\hat{g}_1) &= \int_0^1 \mathbb{E} [|\hat{g}_1(t, x_t, \xi)|^2 - 2x_1 \cdot \hat{g}_1(t, x_t, \xi)] dt, \\ L_z(\hat{g}_z) &= \int_0^1 \mathbb{E} [|\hat{g}_z(t, x_t, \xi)|^2 - 2z \cdot \hat{g}_z(t, x_t, \xi)] dt, \end{aligned} \quad (7)$$

where \mathbb{E} denotes an expectation over $(x_0, x_1) \sim \rho(x_0, x_1|\xi)$, $\xi \sim \eta(\xi)$, and $z \sim \mathbf{N}(0, Id)$.

Proof. By definition of the stochastic interpolant given in (1), its characteristic function is given by

$$\mathbb{E}[e^{ik \cdot x_t}] = \int_{\mathbb{R}^d \times \mathbb{R}^d} e^{ik \cdot (\alpha(t)x_0 + \beta(t)x_1)} \rho(x_0, x_1|\xi) dx_0 dx_1 e^{-\frac{1}{2}\gamma^2(t)|k|^2}, \quad (21)$$

where we used $z \perp (x_0, x_1)$ and $z \sim \mathbf{N}(0, Id_d)$. The smoothness in k of (21) guarantees that the distribution of x_t has a density $\rho(t, x|\xi) > 0$ globally. By definition of x_t , this density $\rho(t, x|\xi)$ satisfies, for any suitable test function $\phi : \mathbb{R}^d \rightarrow \mathbb{R}$,

$$\int_{\mathbb{R}^d} \phi(x) \rho(t, x|\xi) dx = \int_{\mathbb{R}^d \times \mathbb{R}^d \times \mathbb{R}^d} \phi(x_t) \rho(x_0, x_1|\xi) (2\pi)^{-d/2} e^{-\frac{1}{2}|z|^2} dx_0 dx_1 dz. \quad (22)$$

Above, $x_t = \alpha(t)x_0 + \beta(t)x_1 + \gamma(t)z$. Taking the time derivative of both sides

$$\begin{aligned} & \int_{\mathbb{R}^d} \phi(x) \partial_t \rho(t, x|\xi) dx \\ &= \int_{\mathbb{R}^d \times \mathbb{R}^d \times \mathbb{R}^d} (\dot{\alpha}(t)x_0 + \dot{\beta}(t)x_1 + \dot{\gamma}(t)z) \cdot \nabla \phi(x_t) \rho(x_0, x_1|\xi) (2\pi)^{-d/2} e^{-\frac{1}{2}|z|^2} dx_0 dx_1 dz \\ &= \int_{\mathbb{R}^d} \mathbb{E} [(\dot{\alpha}(t)x_0 + \dot{\beta}(t)x_1 + \dot{\gamma}(t)z) \cdot \nabla \phi(x_t) | x_t = x] \rho(t, x|\xi) dx \\ &= \int_{\mathbb{R}^d} \mathbb{E} [\dot{\alpha}(t)x_0 + \dot{\beta}(t)x_1 + \dot{\gamma}(t)z | x_t = x] \cdot \nabla \phi(x) \rho(t, x|\xi) dx \end{aligned} \quad (23)$$

where we used the chain rule to get the first equality, the definition of the conditional expectation to get the second, and the fact that $\phi(x_t) = \phi(x)$ conditioned on $x_t = x$ to get the third. Since

$$\mathbb{E} [\dot{\alpha}(t)x_0 + \dot{\beta}(t)x_1 + \dot{\gamma}(t)z | x_t = x] = \dot{\alpha}(t)g_0(t, x, \xi) + \dot{\beta}(t)g_1(t, x, \xi) + \dot{\gamma}(t)g_z(t, x, \xi) \quad (24)$$

by the definition of g_0 , g_1 , and g_z in (3), we can use the definition of b in (5) to write (23) as

$$\int_{\mathbb{R}^d} \phi(x) \partial_t \rho(t, x|\xi) dx = \int_{\mathbb{R}^d} b(t, x, \xi) \cdot \nabla \phi(x) \rho(t, x|\xi) dx. \quad (25)$$

This equation is (4) written in weak form.

To establish (6), note that if $\gamma(t) > 0$, we have

$$\begin{aligned}\mathbb{E}[ze^{i\gamma(t)k \cdot z}] &= -\gamma^{-1}(t)(i\partial_k)\mathbb{E}[e^{i\gamma(t)k \cdot z}], \\ &= -\gamma^{-1}(t)(i\partial_k)e^{-\frac{1}{2}\gamma^2(t)|k|^2}, \\ &= i\gamma(t)ke^{-\frac{1}{2}\gamma^2(t)|k|^2}.\end{aligned}\tag{26}$$

As a result, using $z \perp (x_0, x_1)$, we have

$$\mathbb{E}[ze^{ik \cdot x_t}] = i\gamma(t)k\mathbb{E}[e^{ik \cdot x_t}].\tag{27}$$

Using the properties of the conditional expectation, the left-hand side of this equation can be written

$$\begin{aligned}\mathbb{E}[ze^{ik \cdot x_t}] &= \int_{\mathbb{R}^d} \mathbb{E}[ze^{ik \cdot x_t} | x_t = x] \rho(t, x | \xi) dx, \\ &= \int_{\mathbb{R}^d} \mathbb{E}[z | x_t = x] e^{ik \cdot x} \rho(t, x, \xi) dx, \\ &= \int_{\mathbb{R}^d} g_z(t, x, \xi) e^{ik \cdot x} \rho(t, x, \xi) dx,\end{aligned}\tag{28}$$

where we used the definition of g_z in (3) to get the last equality. Since the right-hand side of (27) is the Fourier transform of $-\gamma(t)\nabla\rho(t, x|\xi)$, we deduce that

$$g_z(t, x, \xi)\rho(t, x|\xi) = -\gamma(t)\nabla\rho(t, x|\xi) = -\gamma(t)\nabla\log\rho(t, x|\xi)\rho(t, x|\xi).\tag{29}$$

Since $\rho(t, x|\xi) > 0$, this implies (6) when $\gamma(t) > 0$.

Finally, to derive (7), notice that we can write

$$\begin{aligned}L_0(\hat{g}_0) &= \int_0^1 \mathbb{E}[|\hat{g}_0(t, x_t, \xi)|^2 - 2x_0 \cdot \hat{g}_0(t, x_t, \xi)] dt, \\ &= \int_0^1 \int_{\mathbb{R}^d} \mathbb{E}[|\hat{g}_0(t, x_t, \xi)|^2 - 2x_0 \cdot \hat{g}_0(t, x_t, \xi) | x_t = x] \rho(t, x | \xi) dx dt \\ &= \int_0^1 \int_{\mathbb{R}^d} [|\hat{g}_0(t, x_t, \xi)|^2 - 2\mathbb{E}[x_0 | x_t = x] \cdot \hat{g}_0(t, x, \xi)] \rho(t, x | \xi) dx dt \\ &= \int_0^1 \int_{\mathbb{R}^d} [|\hat{g}_0(t, x_t, \xi)|^2 - 2g_0(t, x, \xi) \cdot \hat{g}_0(t, x, \xi)] \rho(t, x | \xi) dx dt\end{aligned}\tag{30}$$

where we used the definition of g_0 in (3). The unique minimizer of this objective function is $\hat{g}_0(x_t, \xi) = g_0(t, x, \xi)$, and we can proceed similarly to show that the unique minimizers of $L_1(\hat{g}_1)$ and $L_z(\hat{g}_z)$ are $\hat{g}_1(x_t, \xi) = g_1(t, x, \xi)$ and $\hat{g}_z(x_t, \xi) = g_z(t, x, \xi)$, respectively. \square

Corollary 3 (Probability flow and diffusions). *The solutions to the probability flow equation*

$$\dot{X}_t = b(t, X_t, \xi)\tag{9}$$

enjoy the property that

$$X_{t=1} \sim \rho_1(x_1 | \xi) \quad \text{if} \quad X_{t=0} \sim \rho_0(x_0 | \xi)\tag{10}$$

$$X_{t=0} \sim \rho_0(x_0 | \xi) \quad \text{if} \quad X_{t=1} \sim \rho_1(x_1 | \xi)\tag{11}$$

In addition, for any $\epsilon(t) \geq 0$, solutions to the forward SDE

$$dX_t^F = b(t, X_t^F, \xi)dt - \epsilon(t)\gamma^{-1}(t)g_z(t, X_t^F, \xi)dt + \sqrt{2\epsilon(t)}dW_t,\tag{12}$$

enjoy the property that

$$X_{t=1}^F \sim \rho_1(x_1 | \xi) \quad \text{if} \quad X_{t=0}^F \sim \rho_0(x_0 | \xi),\tag{13}$$

and solutions to the backward SDE

$$dX_t^R = b(t, X_t^R, \xi)dt + \epsilon(t)\gamma^{-1}(t)g_z(t, X_t^R, \xi)dt + \sqrt{2\epsilon(t)}dW_t,\tag{14}$$

enjoy the property that

$$X_{t=0}^R \sim \rho_0(x_0 | \xi) \quad \text{if} \quad X_{t=1}^R \sim \rho_1(x_1 | \xi).\tag{15}$$

Proof. The probability flow ODE is the characteristic equation of the transport equation (4), which proves the statement about its solutions X_t . To establish the statement about the solution of the forward SDE (12), use expression (6) for $\nabla \log \rho(t, x, \xi)$ together with the identity $\Delta \rho(t, x, \xi) = \nabla \cdot (\nabla \log \rho(t, x, \xi) \rho(t, x, \xi))$ to write (4) as the forward Fokker-Planck equation

$$\partial_t \rho(t, x|\xi) + \nabla \cdot ((b(t, x, \xi) - \epsilon(t)\gamma^{-1}(t)g_z(t, x, \xi))\rho(t, x|\xi)) = \epsilon(t)\Delta \rho(t, x|\xi) \quad (31)$$

to be solved forward in time since $\epsilon(t) > 0$. To establish the statement about the solution of the reversed SDE (14), proceed similarly to write (4) as the backward Fokker-Planck equation

$$\partial_t \rho(t, x|\xi) + \nabla \cdot ((b(t, x, \xi) + \epsilon(t)\gamma^{-1}(t)g_z(t, x, \xi))\rho(t, x|\xi)) = -\epsilon(t)\Delta \rho(t, x|\xi) \quad (32)$$

to be solved backward in time since $\epsilon(t) > 0$.

□

B FURTHER EXPERIMENTAL DETAILS

Architecture For the velocity model we use the U-net from Ho et al. (2020b) as implemented in [lucidrain’s denoising-diffusion-pytorch](#) repository; this variant of the architecture includes embeddings to condition on class labels. We use the following hyperparameters:

- Dim Mults: (1,1,2,3,4)
- Dim (channels): 256
- Resnet block groups: 8
- Learned Sinusoidal Cond: True
- Learned Sinusoidal Dim: 32
- Attention Dim Head: 64
- Attention Heads: 4
- Random Fourier Features: False

Image-shaped conditioning in the Unet For image-shaped conditioning, we follow Ho et al. (2022a) and append upsampled low-resolution images to the input x_t at each time step to the velocity model. We also condition on the missingness masks for in-painting by appending them to x_t .

Optimization . We use Adam optimizer (Kingma & Ba, 2014), starting at learning rate $2e-4$ with the StepLR scheduler which scales the learning rate by $\gamma = .99$ every $N = 1000$ steps. We use no weight decay. We clip gradient norms at 10,000 (this is the norm of the entire set of parameters taken as a vector, the default type of norm clipping in PyTorch library).

Integration for sampling We use the Dopri solver from the torchdiffeq library (Chen, 2018).

Miscellaneous We use Pytorch library along with Lightning Fabric to handle parallelism.

Below we include additional experimental illustrations in the flavor of the figures in the main text.

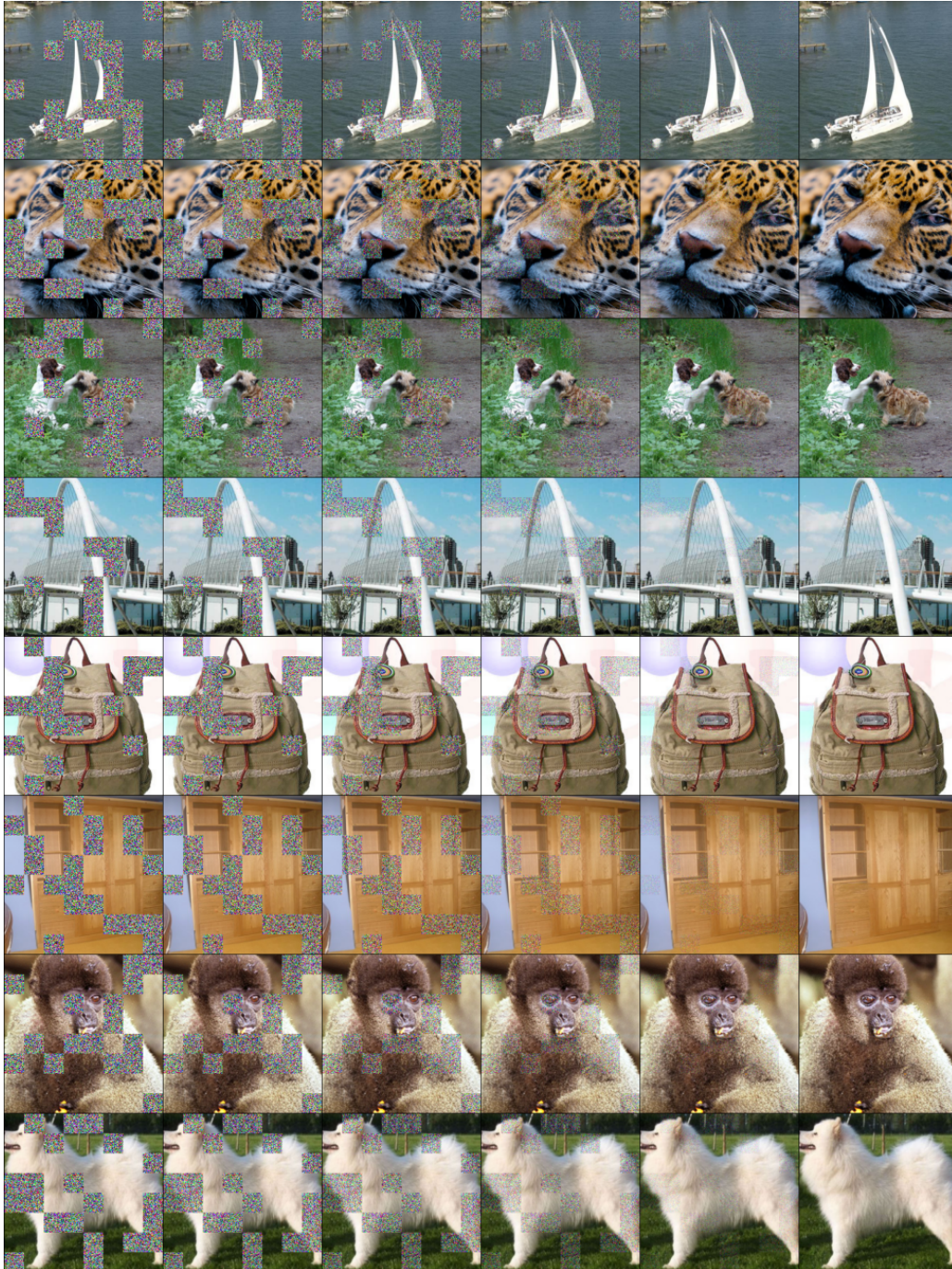


Figure 7: Additional examples of in-filling on the 256×256 resolution images, with temporal slices of the probability flow.

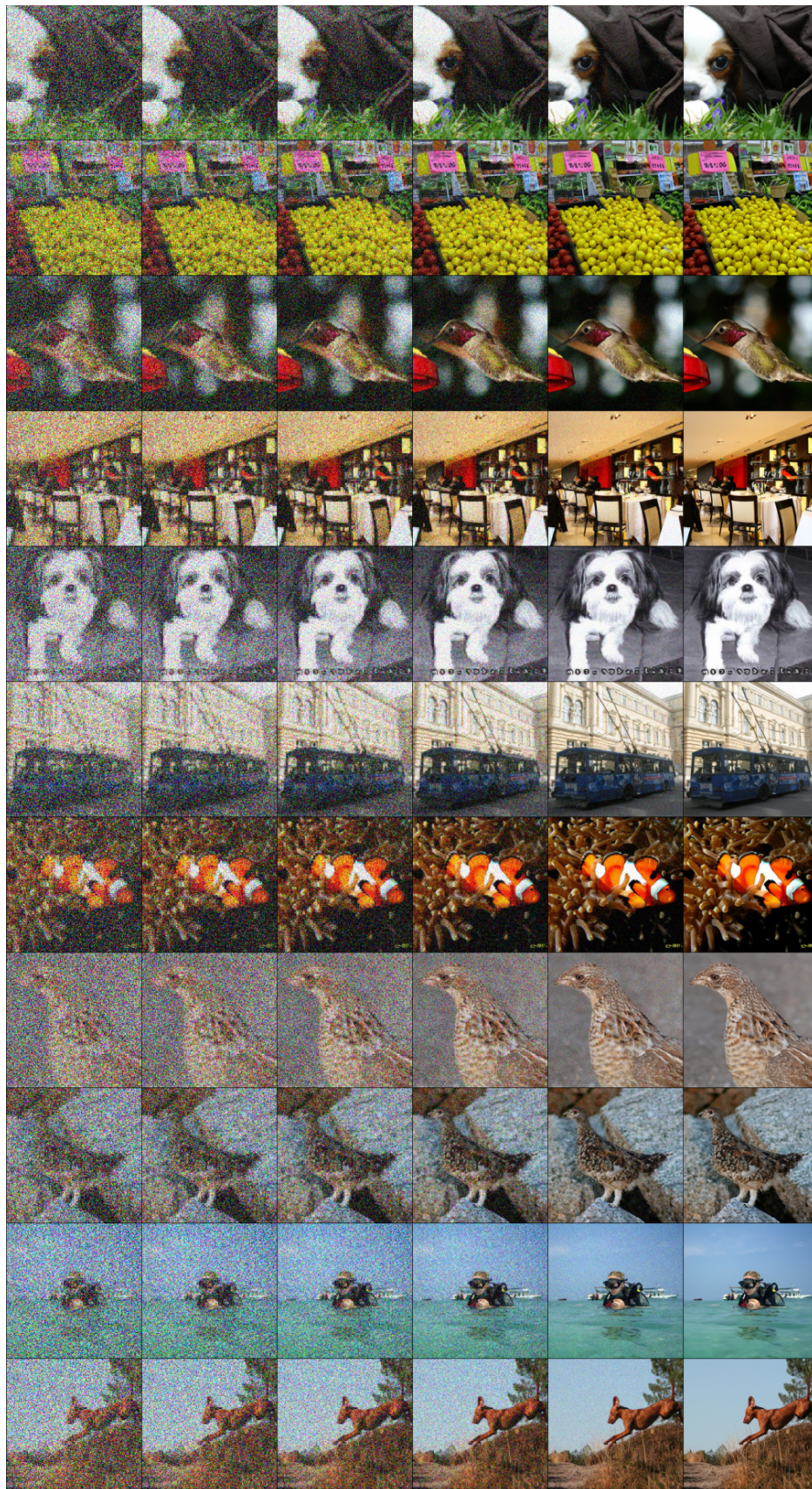


Figure 8: Additional examples of super-resolution from 64 to 256, with temporal slices of the probability flow.